

The Average Relative Entropy and Transpilation Depth determines the noise robustness in Variational Quantum Classifiers.

1st Aakash Ravindra Shinde
Department of Computer Science
University of Helsinki
Helsinki, Finland
shinde.aakashravindra@helsinki.fi

2nd Arianne Meijer - van de Griend
Department of Computer Science
University of Helsinki
Helsinki, Finland
arianne.vandegriend@helsinki.fi

3rd Jukka K. Nurminen
Department of Computer Science
University of Helsinki
Helsinki, Finland
jukka.k.nurminen@helsinki.fi

Abstract—Variational Quantum Algorithms (VQAs) have been extensively researched for applications in Quantum Machine Learning (QML), Optimization, and Molecular simulations. Although designed for Noisy Intermediate-Scale Quantum (NISQ) devices, VQAs are predominantly evaluated classically due to uncertain results on noisy devices and limited resource availability. Raising concern over the reproducibility of simulated VQAs on noisy hardware. While prior studies indicate that VQAs may exhibit noise resilience in specific parameterized shallow quantum circuits, there are no definitive measures to establish what defines a shallow circuit or the optimal circuit depth for VQAs on a noisy platform. These challenges extend naturally to Variational Quantum Classification (VQC) algorithms, a subclass of VQAs for supervised learning. In this article, we propose a relative entropy-based metric to verify whether a VQC model would perform similarly on a noisy device as it does on simulations. We establish a strong correlation between the average relative entropy difference in classes, transpilation circuit depth, and their performance difference on a noisy quantum device. Our results further indicate that circuit depth alone is insufficient to characterize shallow circuits. We present empirical evidence to support these assertions across a diverse array of techniques for implementing VQC, datasets, and multiple noisy quantum devices.

Index Terms—Variational Quantum Classifier, Quantum Machine Learning, Quantum Relative Entropy, Noise Resilient Quantum Circuits, Shallow Circuits

I. INTRODUCTION

Variational Quantum Algorithms (VQAs) have emerged as a promising approach for Noisy Intermediate-Scale Quantum (NISQ) devices for their potential noise-resilience and their adaptability to a wide range of problems [1]. In the context of machine learning, especially for classification tasks, it takes several forms of Variational Quantum Classifiers (VQCs). While extensive research has been conducted to enhance these algorithms, their implementation often relies on simulations in noise-free environments using classical hardware. This raises concerns about the reproducibility of results on actual quantum hardware. Although VQAs exhibit noise tolerance in shallow circuits [2], there is no definition of circuit shallowness, nor a systematic framework to predict when simulated performance translates to noisy hardware. Addressing this gap is essential

for the reliable deployment of VQCs in real-world quantum systems.

Several challenges arise when training or testing VQAs on noisy quantum devices. Noise significantly impacts the overall implementation and skews the results for any Quantum Circuit implementation [3]. VQAs are hybrid quantum-classical algorithms, and their training can be challenging due to significant changes in unitary operations for the optimizer [1]. This noise interaction can result in the noise-induced barren plateau problem, where gradients become negligible [4].

Furthermore, running algorithms on quantum hardware while optimizing with classical methods is slow and often hindered by accessibility issues like high costs and long wait times for each iteration [5]. Since VQAs need multiple iterations to find optimal solutions, these approaches can be economically inefficient.

Using noisy quantum hardware to validate simulated models often yields disappointing or unclear results due to model variations. Additional concerns with variational quantum algorithms (VQAs) include scalability and the barren plateau issue during training. These factors may suggest that VQAs are inconsequential in the development of quantum algorithms.

However, research has indicated that VQAs could be noise-resilient and particularly useful for NISQ (Noisy Intermediate-Scale Quantum) devices [2]. Despite these findings, discrepancies have emerged in empirical executions on NISQ devices; some quantum circuits perform well, while others do not [6]. Another advantage of VQCs is their tolerance to a certain level of uncertainty in results. While algorithms that demand extreme precision struggle in this regard, the probabilistic design of VQC models accommodates some level of uncertainty and is even welcomed in certain cases of machine learning implementation. Nonetheless, significant uncertainty in VQC models can still lead to inaccurate outcomes.

Looking into the pros and cons of VQAs, we address the following questions in this manuscript. What makes some shallow quantum circuits display noise resilience during experimentation, while others with the same transpilation depth do

not? Secondly, is it possible to verify if a classically simulated and trained quantum classification algorithm would perform equivalently in a noisy setting, and can it be known without full noisy executions? Finally, can this determination of noisy resilience verification lead to scalable VQAs?

Answering the posed questions, we have resulted in the following list of contributions from this research:

- We propose a classical evaluation procedure to determine the reproducibility of Variational Quantum models on a noisy quantum device based on the average relative entropy between classes and transpilation depth.
- We present an analytical explanation for the noise-resilience of a certain shallow circuit under similar depth and architecture.
- We conduct a detailed evaluation of the procedure through extensive experimentation, considering a variety of parameters. This includes different ansatzes, model implementations, datasets, and measurement techniques across various quantum devices from different providers. Each device consists of diverse transpilation methods, qubit mapping strategies, gate sets, noise levels, and architectural configurations, allowing us to cover multiple possible scenarios comprehensively.

This manuscript is structured as follows. Section II discusses former work in the fields of Variational algorithms, Relative Entropy, and noise. This section also provides a brief reasoning for the pursuit of this research. In the following, Section III we discuss the experimental components and in section IV we discuss the experimental process associated with those components. In Section V we present our findings, which are further analyzed in Section VI. Finally, we present our conclusion in Section VII with continuations for future work in Section VIII.

II. BACKGROUND

This section summarizes prior research on the noisy execution of Variational Quantum Algorithms and their inter-reliability using relative entropy measures. We highlight evidence showing that Variational Circuits can be noise robust in certain cases, alongside research indicating the negative impact of noise on these circuits. Additionally, we address findings on the deterioration of relative entropy in noise channels and our observations on using average relative entropy as a reproducibility measure.

Sharma et al. (2020) [2] claim that VQAs, especially Full Matrix Compiling (FMC) and Fixed Input State Compiling (FISC), are resilient to measurement and depolarization noise, supported by theoretical insights and numerical results across various hardware. They attribute this resilience to a general unitary transformation, but do not explore the parameterized resilience to coherent noise, leaving training, accuracy, and overall noise resilience unexamined. Fontana et al. (2021) [7] analyze short quantum circuit simulations across different noise models, noting that the impact on VQE increases with circuit depth. In contrast, Khanal et al. (2023) [6] report effects

of noise on various ansatz designs and dataset complexities, without clear explanations for observed discrepancies.

Ahmed et al. (2025) [8] conducted similar experimental research on QNN models to analyze the effects of noise. They aimed to explain the QNN model’s resilience to simulated noise through measurement probability distribution. However, our results contradict their argument that some models perform similarly regardless of the distribution.

Alternatively, the downsides of noise on VQAs have been discussed in several articles before, which predominantly lie with the parameter shift due to noise during training, leading to noise-induced barren plateau [4]. Similarly, Barligea et al. (2025) [9] presented research involving VQE and QAOA algorithms under stochastic noise and raised concerns regarding the scalability of VQE algorithms under such conditions. In Cerezo et al. (2021) [1], the authors mention the idea of noise accumulation and its association with depth in a VQC without a clear discerning way to determine the ideal depth for a shallow circuit.

Error detection techniques [10] and error mitigation techniques [11] have been researched for noisy VQA executions, but this has raised concerns regarding the quality of the ancillary system and the scalability of applied methods. Hence, a method that determines the working of a Variational Algorithm in a noisy hardware environment could significantly enhance the usability of VQC algorithms.

An important proof presented in De Palma et al. (2023) [11] shows that the relative entropy decreases as it passes through a noisy channel. This establishes a congruence between relative entropy, noisy circuit depth, and accuracy of the final state.

Entropy is a highly versatile concept in quantum information; this is also evident in VQAs. The entropy concept is prominently used as a cross-entropy cost function in Variational Quantum Classifiers, akin to classical neural networks. This loss function evaluates model performance by measuring output probabilities and analyzing measurement probabilities in single-qubit states [12]. Mondal et al. (2025) [13] used relative entropy in Quantum Neural Networks to measure divergence between learned and target states, improving training stability against CPTP depolarizing noise. Tsuda et al. (2009) demonstrated that the matrix-exponentiated gradient update, inspired by quantum relative entropy, has applications in classical machine learning for establishing an upper bound on total loss for the proposed online algorithm in [14]. The quantum relative entropy plays a significant role in the Quantum Boltzmann Machine, another aspect of QML, as an intuitive way to measure the quality of the approximation [15].

Variational Quantum Circuits have been employed to estimate Von Neumann entropy, Rényi entropies, and Quantum Mutual Information. Researchers in Goldfeld et al. [16] developed a quantum neural estimation algorithm that utilizes parameterized quantum circuits and classical neural networks to efficiently approximate various quantum information measures through sampling and optimization. Concurrently, another study [17] introduced Quantum Mutual Information Neural Estimation (QMINE), which leverages quantum neural

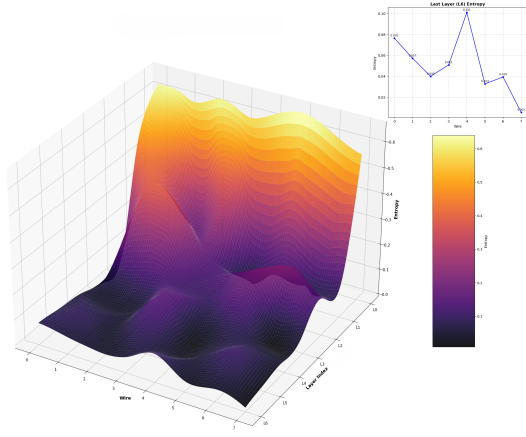


Fig. 1:

Average relative entropy for data exhibiting the same measurement value across each layer and qubit, with Wire 7 being the measurement qubit. The graph on top represents the entropy values in the last layer for all qubits.

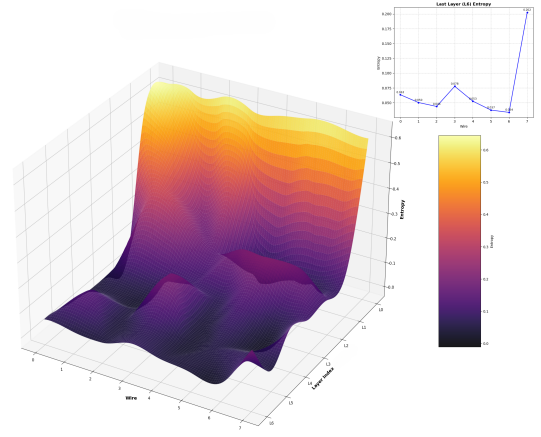


Fig. 2:

Average relative entropy for data exhibiting the different measurement value across each layer and qubit, with Wire 7 being the measurement qubit. The graph on top represents the entropy values in the last layer for all qubits.

networks to minimize a loss function for Von Neumann entropy and quantum mutual information, utilizing a quantum version of the Donsker-Varadhan representation (QDVR).

We further explored the relationship between relative entropy and variational quantum classification circuits to better understand information flow within a quantum circuit. During our initial investigation, we identified two key observations that inspired the method proposed in this article. We calculated the relative entropy for each qubit in relation to the final measurement qubit for each layer. The results are illustrated in Fig. 1, which compares the average relative entropy for data exhibiting the same measurement value, and in Fig. 2, which compares the average relative entropy for data with opposite measurement values.

The observations from Figures Fig. 1 and Fig. 2 reveal that in a Variational Circuit, the entropy value decreases from the beginning to the end of a quantum circuit. Additionally, the relative entropy between opposite measurement states is significant only at the measurement qubits, as observed on Wire 7 and Layer 6 in both figures. These findings, combined with previous research by De Palma et al. (2023) on the reduction of relative entropy in a noisy channel [11], prompted us to explore the effects of noisy executions on Variational Quantum Circuits (VQCs) by analyzing the Average Relative Entropy between classes.

In this manuscript, we expand our research for finding an association between noise, depth, and average relative entropy based on observations regarding the average relative entropy amongst classes, noise resilience in shallow depth circuits, and depleting relative entropy in a noise channel. We also intended to investigate whether this procedure could be deduced without explicitly evaluating on noisy hardware. We provide extensive empirical experimentation for building this association across various noisy backends and variational structures.

III. EXPERIMENTAL COMPONENTS

To be thorough with the empirical studies, considering the several ways in which variational classifiers could be defined, we restricted ourselves to binary classification problems with 8-qubit circuits, so that we can investigate a wide set of parameters for a generalizable result.

Considering the different ways to represent and create variational classifiers, we evaluated three major ways in which variational circuits are implemented. Since there is no intuitive method to determine which quantum ansatzes and data encoding methods are appropriate for specific problems, we employed over 20 distinct quantum ansatz structures and 5 ways for data encoding. Additionally, we examined several other ansatz representations to identify commonalities with other quantum algorithms, as discussed in section XI. As the result should not be data dependent, these models were trained on five different datasets chosen based on their complexity and variance from one another. Parameters for datasets were trained with random parameters at initialization. We used several different optimizers, such as Nesterov Momentum, Adam, Gradient Descent, and AdaGrad, with some novel variations in training as discussed in Section IV, as well as several different cost functions, such as mean absolute error, hinge loss, cross entropy, and square loss. Considering how all variational circuits were initialized at random, we trained all combinations at least five times. To eliminate doubts that these methods are only effective for a specific accuracy value range, we selected several models with an accuracy higher than 85% for further evaluation.

This section offers a comprehensive overview of all the experimental components utilized in the procedure. The following section will outline how these components were implemented in the overall experiment. A detailed discussion of the experimental components is presented as follows:

A. Variational Quantum Machine Learning

Variational quantum circuits have been extensively studied in quantum machine learning. These circuits can be expressed in the form $f(\theta, x) = \text{Tr}[O(x, \theta)\rho(x, \theta)]$, where x represents the input data points, O denotes observable parameters, ρ is the density matrix, and θ is the adjustable parameter.

To train these models, a differentiable cost function is defined as $L(\theta, X, y) = \frac{1}{N} \sum_i l(\theta, x_i, y_i)$. Here, the loss $l(\theta, x_i, y_i)$ quantifies the model's performance for a specific training data point x_i , for which the true label y_i is known. Let matrices X and y summarize all training inputs and labels, respectively [18].

Similar to the classical neural network training procedure, the loss is numerically minimized using a classical optimizer over each iteration and batch of data values. Optimizer for each iteration updates the rotational parameters to reduce the loss value [18]. For this experimentation, we have considered several kinds of structure, some with repeating 2-qubit ansatzes and some confined to a static structure. The 8 qubits ansatz structure was inspired by the works presented in Hubregtsen et. al. (2021) [19], Hur et. al. (2022) [12], and Sim et. al. (2019) [20]. We classified these structures into three major ways of implementing the QML algorithm for this experimentation. These are classified based on an implementational naming convention as per the structures and not based on any other way of classifying methods.

1) *Parameterized or Variational Quantum Circuits (PQC/VQC)*: Here, we define Parameterized Quantum Circuit (PQC)-based models as multi-layered ansatzes composed of both single and two-qubit quantum gates, without subsequent reduction of qubit operations. The depth of these circuits can be enhanced through the repetition of gate structures, tailored to meet the complexity requirements of the model, thus yielding improved performance outcomes. Data encoding structure is appended once at the beginning of the structure.

While increasing the repetition of the ansatzes enhances the expressibility of PQC models, it also leads to an increase in circuit depth and associated implementational constraints. This trade-off between expressibility and practicality is a critical aspect to consider in designing PQC models.

2) *Quantum Neural Networks (QNN)*: QNNs are inherently similar to PQCs, with one key structural difference between PQCs and QNNs being that in QNNs, as depicted in [12], the ansatzes acting on all qubits are halved with each layer, ultimately leading to the measurement of the remaining qubit.

QNNs have a reduced number of operational ansatzes compared to PQCs/VQCs, which helps decrease the overhead associated with circuit implementation. They have also been shown to significantly reduce the issues related to the Barren Plateau problem during the training phase. However, there are ongoing questions about the ease of simulating such structures and the expressibility of these models [21].

3) *Data Re-upload*: Data re-uploading involves repeatedly encoding classical data into quantum circuits, which can significantly improve the expressiveness of quantum models without a substantial increase in computational requirements.

The process of data re-uploading is accomplished by linking together repeated units of tunable PQCs and Static Data encoding circuits in a sequence. Consequently, a quantum circuit can be structured as a combination of data re-uploading and single-qubit processing units. Several recent studies suggest that data re-uploading can enhance the performance and trainability of quantum models [22].

B. Average Relative Entropy between a set of states

Before defining Average Relative Entropy between a set of states, we first examine the definition of Quantum Relative Entropy (Von Neumann relative entropy) between a density operator $\rho \in \mathcal{D}(\mathcal{H})$ and a positive semi-definite operator $\sigma \in \mathcal{L}(\mathcal{H})$. It is defined as,

$$\mathcal{D}(\rho||\sigma) \equiv \text{Tr}\rho[\log \rho - \log \sigma], \quad (1)$$

if the $\text{supp}(\rho) \subseteq \text{supp}(\sigma)$ [23]. This measure has the same statistical interpretation as the classical relative entropy: it quantifies the distinguishability between the two quantum states ρ and σ . The quantum relative entropy is an important quantity in classifying and quantifying correlations. The quantum relative entropy is 0 when $\rho = \sigma$.

Here, the Average Relative Entropy between two classes for a binary classification (Label 1 or Label 2) VQC model U is defined as follows:

$$\mathcal{D}_{avg}(\rho||\sigma) = \frac{1}{n+m} \sum_{i,j=0}^{n,m} \mathcal{D}(U\rho_i U^\dagger || U\sigma_j U^\dagger) \quad (2)$$

where $i \in \{0, n\}$ for n values in a set, $j \in \{0, m\}$ for m values in a set, $\rho_i = |\psi_i\rangle\langle\psi_i|$ and $\sigma_j = |\phi_j\rangle\langle\phi_j|$ are density matrix representation for all data values after classical to quantum embedding for their respective label class.s. From our experimentation we observe, $\mathcal{D}_{avg}(\rho||\sigma) \approx \mathcal{D}_{avg}(\sigma||\rho)$.

C. Dataset Generation Methods

For extensive evaluation, datasets with varying complexities and intricacies are essential. Hence, we employed five different methods for dataset generation, each with its own prediction difficulties. For each data generation, we kept the modifiable parameters constant, maintaining significant complexities. The first two of the dataset generators are chosen for their ability to generate Gaussian and non-Gaussian distributions, respectively. While the final three are inspired by the benchmarking initiative in [18].

1) *Make Classification by Scikit-Learn (Linear Dataset Creator)*: The algorithm for the Make Classification function is based on the concept in [24] and was developed to create the "Madelon" dataset. This function is particularly effective at introducing noise through attributes like correlated, redundant, and uninformative features. Additionally, it generates noise by forming multiple Gaussian clusters within each class and applying linear transformations to the feature space [25].

2) Synthetic Data by Capital One (Non-linear Dataset):

The Synthetic Data generator is a tool for creating tabular datasets that incorporate non-linearity using a Non-Gaussian distribution. The feature set generated is tunable over three parameters: informative, redundant, and nuisance. Informative parameters generate features crucial for determining binary labels, which are defined using Copula theory, a mathematical approach that separates the correlation structure from the marginal distributions of the feature vectors. The Redundant parameter helps create a linear combination of the informative features, while nuisance features help generate features consisting of uncorrelated vectors drawn from the range $[-1,1]$. For more details about the dataset, please refer to [26].

3) *Hidden Manifold*: Goldt et al. [27] introduced a data generation procedure designed to explore the impact of data structure, such as the size of a hidden manifold believed to influence problem difficulty, on learning outcomes. The process involves generating inputs on a low-dimensional manifold, which are then labeled by a simple, randomly initialized neural network. Finally, these inputs are projected into a d -dimensional space [18].

4) *Hyperplanes*: This data generation method creates several hyperplanes in a k -dimensional space and assigns labels to randomly sampled points based on the parity of perceptron classifiers using these hyperplanes as decision boundaries. A label indicates whether a point is on the positive side of an even number of hyperplanes, aiming to reflect the "global" structure of the problem related to the arrangement of hyperplanes [18].

5) *Two Curves*: This data generation procedure is inspired by a theoretical study, as discussed in et al. [28], which demonstrates how the performance of neural networks is affected by the curvature and the distance between two one-dimensional curves embedded in a higher-dimensional space. Following the implementation in [18], we also used low-degree Fourier series to embed two sets of data sampled from a one-dimensional interval, with one set for each class, representing these data as curves in d -dimensional space, while also adding some Gaussian noise.

D. Data Encoding

Data encoding is a key element of Quantum Machine Learning (QML). Unlike classical methods that use vectors, QML requires transforming classical data into quantum states through encoding circuits. These circuits are referred to as quantum feature maps or quantum encodings, also interchangeably known as embeddings. The encoding process significantly affects QML model performance, so choosing the right encoding method for the dataset is essential [29]. We have utilized the most commonly used encoding methods for Variational Quantum Classification models in our work.

1) *Angle Encoding*: One of the most common encoding methods involves representing data values for each feature as an angle of rotation along different axes: X, Y, or Z. This is expressed mathematically as $R_j(\theta) = e^{-i\frac{\theta}{2}\sigma_j}$, where $j \in \{x, y, z\}$ and σ_j represents the Pauli matrices $\sigma_x, \sigma_y, \sigma_z$. In

this encoding method, N feature values are embedded into N qubits [30]. For our experimentation, we have tested for all three rotational values across all variational circuits in this manuscript.

2) *Amplitude Encoding*: In the case of Amplitude encoding, classical feature vectors are represented as amplitudes. Here, classical feature vector $x = \{x_1, \dots, x_n\}$ can be written as $|\psi\rangle = \sum_{i=1}^n x_i |i\rangle$, where $|\psi\rangle$ is the resulting quantum state and $|i\rangle$ are the quantum state for each vector components for i being the binary index of values. An N -dimensional amplitude encoded classical vector requires $\log_2 N$ qubits. Considering the expensive circuit implementation of state initialization, evaluation of amplitude encoding was essential in understanding the bottleneck of QML implementation [30].

3) *Instantaneous Quantum Polynomial (IQP) Encoding*: The instantaneous Quantum Polynomial-time (IQP) encoding maps features into qubits via diagonal gates in an IQP circuit. An IQP circuit is a type of quantum circuit that consists of a sequence of Hadamard gates followed by a sequence of diagonal gates in the computational basis. In this context, the diagonal gates are single-qubit R $_z$ rotations applied to each qubit, encoding the n features. This is followed by two-qubit ZZ entanglers, represented as $e^{-ix_i x_j \sigma_z \otimes \sigma_z}$. This method is capable of encoding N data points into N qubits [31].

E. Measurements

Measurement in a quantum system involves retrieving information [32]. In the context of a classification Quantum Machine Learning (QML) system, the focus is on measuring quantum circuits to extract information based on quantum-encoded classical data. This process helps us determine the class for a specific set of labels.

For binary classification problems, measurements usually involve obtaining information from a single qubit. In the practical implementation of Variational QML algorithms, measurements are often performed probabilistically, where the classes are represented by the labels '0' and '1' [5]. Alternatively, measurements can be made as the expectation value of the system, with the labels corresponding to the eigenvalues '-1' and '1' [33].

1) *Shot-based probabilistic measurement*: A "shot" in a quantum circuit is a single execution that produces probabilistic measurement results of 0 or 1 for each qubit. In Variational Circuits, quantum information is projected into the computational basis, and measurement probabilities are estimated over multiple shots, as several executions are needed for accurate probability estimation.

Although increasing the number of shots improves precision, it also raises resource costs. The statistical error in probability estimation decreases with the square root of the number of shots used. Typically, a default value of 1,024 shots is used, but this can be adjusted according to the desired level of precision.

2) *Expectation Values*: The expectation value is the probabilistic average of the results (or measurements) from an experiment. It represents an average of all possible outcomes,

weighted by their likelihood. However, it is important to note that the expectation value is not necessarily the most probable value of a measurement; in fact, it can even have zero probability.

Given an observable $A = \sum_k \lambda_k |k\rangle \langle k|$, we obtain eigenvalue λ_k with probability p_k , we can naturally define an expectation value of this observable in the state $|\psi\rangle$ as $\langle A_\psi \rangle \equiv \sum_k \lambda_k \langle \psi | P_k | \psi \rangle = \langle \psi | (\sum_k \lambda_k P_k) | \psi \rangle = \langle \psi | A | \psi \rangle = \text{Tr}(A |\psi\rangle \langle \psi|)$ [3]. In our case, as measured in the Z basis, each time we will get +1 or -1.

IV. EXPERIMENTAL PROCEDURE

Experiments were conducted in three phases. In the first phase, models were trained on the datasets generated using methods mentioned in Section III-C under ideal simulation conditions (without noise), and models that achieved an accuracy greater than 85% were selected for the second phase. During the second phase, these models were evaluated on noisy quantum backends using the same testing data as in the previous phase. The third phase involved data analysis, where we examined several factors that could explain the differences in accuracy among various noisy quantum backends for shallow quantum circuits with similar transpilation depths. With extensive analysis, we concluded that the Average Relative Entropy between classes (as computed in Eq. 2) of the quantum circuits best explains the phenomenon.

Phase one of the implementation was carried out entirely using the Pennylane quantum programming framework [34]. We trained five models for each combination of dataset, ansatz, and data encoding method mentioned in Section III. As parameter initialization is random, this approach allowed us to explore which datasets were best suited to specific quantum circuit structures.

We trained more than 2,750 models for the VQC-QNN circuits using shot-biased probabilistic measurement and another 2,750 models for expectation-value measurements. Additionally, we trained 3,000 models for data-reupload circuits with both types of measurements. Each dataset generator produced 5,000 normalized data points, which were then divided into an 80-20 train-test split. During the initial training phase, we observed that using multiple optimizers with varying batch sizes and learning rates in tandem significantly reduced the number of training iterations while achieving respectable accuracy more quickly than using a single optimizer with a fixed batch size and learning rate. Further research on this phenomenon is underway, as discussed in Section VIII.

From the QML models, we selected only those models that achieved an accuracy of over 85% on the test dataset for phase two. This selection resulted in 413 models for the VQC-QNN circuits with probabilistic measurement, 362 models for expectation value measurements, and 400 models for the data-reupload circuits with both measurements. The Puhti Supercomputer was used for training these QML models in a simulated environment, considering the volume of data generation and processing involved.

In phase two, we tested QML models on noisy quantum devices using the same test dataset. Most runs were performed on simulated-fake quantum backends, due to the high costs associated with running experiments on real quantum devices and the extent of data needed for evaluation. These simulations were carried out on the Puhti Supercomputer.

To validate our results, we further tested them on actual quantum devices under several constraints. We employed multiple noisy devices from different vendors to strengthen our findings.

From IBM, we used simulated quantum devices such as 'Sherbrooke,' 'Prague,' 'SydneyV2,' 'JohannesburgV2,' 'MelbourneV2,' 'BoeblingenV2,' 'GuadalupeV2,' 'AlmadenV2,' 'SingaporeV2,' 'Marrakesh,' 'Fez,' and 'Torino.' We confirmed our results with available IBM real quantum devices, specifically Marrakesh, Fez, and Torino, which are currently accessible on the IBM cloud.

From IQM, we utilized simulated quantum devices like Apollo and Aphrodite, both of which have noise models and architectures similar to the real quantum devices Garnet and Emerald, respectively. Additionally, Aphrodite bears resemblance to the Q50 quantum device available at VTT, which was also used for verification.

From IonQ, we worked with the Aria 1 Noisy Quantum Simulator, but we were unable to verify it against the actual Aria 1 device due to restricted access.

Several changes were necessary when executing Pennylane-based circuits on IQM and IonQ devices due to compatibility issues. Hence, we converted the code from Pennylane's compiled tape method into QASM circuits [35]. Subsequently, these QASM circuits were transformed into Qiskit [36] circuits for execution on the respective devices.

In phase three, the data obtained from these noisy backends are evaluated using transpiled depth and average relative entropy between classes. Transpiled depth values are obtained after the quantum circuit is converted into the gate set of the quantum device, using the depth function from the Qiskit implementation. Average relative entropy calculations are computed using the test datapoints for the independent classes.

Results obtained from the analysis in phase three are provided in the next section. We have also provided a graph that showcases the correlation between accuracy difference, average relative entropy, and transpilation depth for different quantum devices.

V. RESULTS

Table I summarizes the results from our experiments, showcasing 51 distinct data points that represent similar observations across different models, encodings, and ansatzes. The results in the table consist of the relevant quantum devices for which the device provider has a noise model to verify. Table I shows values for individual models. 'Sim. Acc.' indicates the simulated accuracy, 'Ansatz' refers to the circuit structures from Section XI, 'Avg Rel Ent.' is the average relative entropy between binary classes as explained in Eq.

2, 'Encoding' denotes data encoding methods, and 'Model' describes circuit structures and measurement types from Section IV. The remaining columns provide details for test set accuracy (Acc.) and transpilation depth (Depth) of circuits on the noisy quantum backend.

Values shown in green indicate that the accuracy of the noisy device differs from the accuracy of the simulation by less than 0.03. Values in red represent an accuracy difference greater than 0.08, while values with accuracy differences between 0.03 and 0.08 are shown in blue. The value difference over multiple runs for the same test data and the same device does not differ more than ± 0.001 in Table I.

We had explored several methods, including quantum circuit complexities, classical to quantum data encoding, relative entropy distribution in quantum circuits across different layers, dataset complexities, the probability distribution of measured values, mutual information between measured and unmeasured qubits, Quantum Rényi divergence, Noisy device attributes such as T1, T2, readout error values, and the characteristics of noisy device gate sets.

Among all these methods, we found a strong correlation between the accuracy differences observed between simulations and noisy devices, the Average Relative Entropy between classes (as computed in Eq. 2), and the transpilation depth of quantum circuits before implementation on the respective noisy quantum hardware. From Table I, it is clear that there is no clear correlation between accuracy and either depth or average relative entropy by themselves as well. However, upon further evaluation, we find a correlation between the accuracy difference vs. depth and the average relative entropy. This relationship is better illustrated with the graphs in Fig. 3 and Fig. 4.

Figures, Fig. 3 and Fig. 4 show plots of accuracy versus log-DTSAE (log of depth to square-root of average relative entropy), defined as $\log\left(\frac{\text{depth}}{\sqrt{\text{avg_rel_ent}}}\right)$, based on over 1,100 analyzed models. The trends are similar across all backends, though the specific log-DTSAE values differ. The blue line indicates the point with the highest instance count, showing an accuracy difference of 0.03, while the red line indicates a difference of 0.08. The green GP (Gaussian Process) mean line represents a predicted growth in the accuracy difference concerning log-DTSAE. It uses Gaussian Process Regression (GPR), a non-parametric machine learning technique effective for complex continuous data [37].

As seen in Fig. 3 and Fig. 4, for a 0.03 accuracy difference, the log-DTSAE values are 4.6533 for Fake Fez and 4.6562 for Fake Torino, with similar values for other backends: Fake Prague (4.6466), Fake Marrakesh (4.7875), Fake Sherbrooke (4.719), Fake Apollo (3.8372), and Fake Aphrodite (3.8264). For the 0.08 accuracy difference, divergence occurs at 7.6169 for Fake Fez, with similar progression for other backends: Fake Marrakesh(7.4310), Fake Torino(7.1316), Fake Prague (7.6112), Fake Sherbrooke(6.2366), Fake Apollo(4.4981), and Fake Aphrodite(4.4823).

Due to the large amount of data required to investigate the

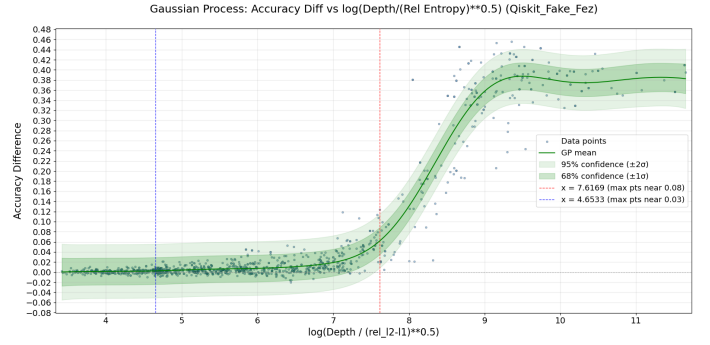


Fig. 3: Average Entropy, Transpilation Depth, and Accuracy difference relation representation using log-DTSAE for Qiskit Fake Fez Backend

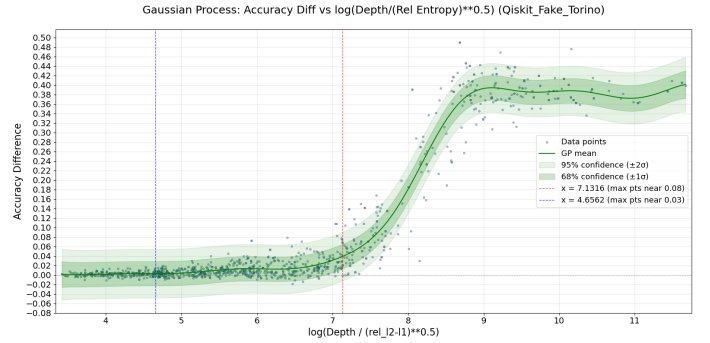


Fig. 4: Average Entropy, Transpilation Depth, and Accuracy difference relation representation using log-DTSAE for Qiskit Fake Torino Backend

factors influencing the decreasing accuracy on noisy backends, it was neither financially nor technically feasible to conduct the full experiment on actual quantum devices. As a result, the use of simulated backends in the experiment was necessary, which was further supported by limited experiments conducted on real quantum devices. We limited our executions to a few models with a smaller verification dataset. We compared results for accessible devices with noisy backends, including Fez(Heron R2), Torino(Heron R1), Marrakesh(Heron R2) from IBM, and Garnet(20 qubits) and Emerald(54 qubits) from IQM, with Emerald sharing architecture with Q50 hosted by VTT.

We had the following constraints when choosing models and data points. Models were selected with varying average relative entropy and similar depth to analyze differences in the previously observed effects. We chose datapoints based on the K-Medoids to find k datapoints that best represent the overall dataset to get an overview of the differences in results across different devices. Results showed that the average variance in readout value for the selected datapoints is under $\Delta 0.03$, proving that the values associated with the noise modeled backends could be observed on the real backends as well. Extending our observations and results to the real noisy devices. More evaluations are in progress for extensive verification. All observations are available for review in the GitHub repositories mentioned in Section X.

Index	Ansatz	Model	Encoding	Avg ReI Ent.	Sim Acc.	Oskit		IOM		IOM		IonQ									
						Fake	Depth	Acc.	Fake	Depth	Acc.	Fake	Depth	Acc.	Fake	Depth	Acc.	Fake	Depth	Acc.	Fake
1	QNN_model_170_pool	VQC_QNN_EXP	AngleY	0.5352	0.892	0.883	62	0.899	62	0.896	62	0.900	66	0.905	99	0.895	99	0.898	131		
2	QNN_H_CZ_RX_pool	VQC_QNN_PROB	Amplitude	0.0881	0.932	0.583	1472	0.692	1604	0.515	1606	0.883	1804	0.883	616	0.883	578	0.883	527		
3	QNN_H_CZ_RX_pool	VQC_QNN_PROB	AngleX	1.5808	0.933	0.932	46	0.931	46	0.935	46	0.932	50	0.934	18	0.930	18	0.934	25		
4	QNN_model_170_pool	VQC_QNN_EXP	IQP	0.2337	0.931	0.928	308	0.918	320	0.923	275	0.932	310	0.913	145	0.838	140	0.924	78		
5	H_CZ_RX	VQC_QNN_EXP	AngleY	0.0245	0.929	0.884	54	0.908	55	0.890	56	0.890	54	0.843	37	0.656	37	0.882	37		
6	QNN_model_170_pool	VQC_QNN_PROB	IQP	0.6240	0.888	0.89	292	0.889	286	0.893	293	0.887	277	0.888	399	0.844	127	0.835	140	0.885	78
7	RY_RZ_CNOT	VQC_QNN_EXP	IQP	0.0351	0.897	0.773	382	0.767	389	0.729	368	0.817	393	0.701	141	0.551	147	0.816	58		
8	RY_CNOT	VQC_QNN_EXP	IQP	0.0191	0.939	0.785	382	0.855	381	0.742	376	0.831	382	0.598	159	0.514	160	0.736	72		
9	RX_RZ_CNOT	VQC_QNN_PROB	AngleX	0.1864	0.947	0.933	67	0.936	67	0.934	67	0.931	67	0.930	90	0.877	36	0.872	36	0.942	24
10	INV_QFT_U3_MODEL	VQC_QNN_PROB	AngleY	0.1217	0.949	0.949	147	0.943	132	0.943	151	0.940	183	0.937	181	0.939	96	0.922	94	0.944	22
11	RY_CZ	VQC_QNN_EXP	Amplitude	0.1710	0.905	0.714	1745	0.744	1974	0.593	1981	0.799	1835	0.545	2406	0.499	714	0.787	594		
12	INV_QFT_U3_MODEL	VQC_QNN_EXP	IQP	0.0956	0.904	0.861	350	0.871	340	0.862	384	0.862	385	0.787	476	0.587	197	0.567	199	0.853	58
13	QNN_RY_CRX_pool	VQC_QNN_EXP	AngleX	1.0540	0.853	0.857	58	0.852	58	0.860	58	0.854	58	0.856	62	0.850	24	0.854	24	0.851	29
14	QNN_model_150params	VQC_QNN_PROB	AngleX	0.6778	0.997	0.995	62	0.997	62	0.999	62	0.999	62	0.997	66	0.995	26	0.995	26	0.995	26
15	QNN_H_CZ_RX_pool	VQC_QNN_EXP	AngleY	0.2083	0.942	0.936	47	0.938	47	0.931	47	0.943	47	0.927	50	0.925	18	0.916	18	0.940	25
16	RX_RZ_CNOT	DATA_REUP_PROB	AngleX	0.1032	0.925	0.927	67	0.919	67	0.919	67	0.919	67	0.907	88	0.859	36	0.850	36	0.908	24
17	RX_RZ_Multi_CRX	DATA_REUP_PROB	AngleX	1.6190	0.955	0.917	1193	0.924	1192	0.907	1150	0.932	1100	0.889	1413	0.654	555	0.653	559	0.930	93
18	RY_RZ_CNOT	DATA_REUP_PROB	AngleX	1.4200	0.947	0.941	162	0.944	171	0.941	134	0.944	173	0.937	239	0.940	22	0.940	22	0.946	21
19	RX_RZ_CRZPool	DATA_REUP_PROB	AngleY	2.5523	0.944	0.942	162	0.944	171	0.940	134	0.943	173	0.940	239	0.942	22	0.934	22	0.941	21
20	H_CZ_RX	DATA_REUP_PROB	Amplitude	1.5761	0.913	0.487	15354	0.456	15606	0.475	15414	0.519	15483	0.508	17811	0.482	6367	0.482	6365	0.500	5102
21	RX_RZ_Multi_CRZ	DATA_REUP_PROB	AngleY	1.1158	0.927	0.926	1124	0.929	2083	0.897	2063	0.918	2172	0.821	2970	0.503	914	0.506	910	0.923	137
22	QNN_RY_CNOT_pool	VQC_QNN_EXP	AngleY	1.6222	0.966	0.965	62	0.963	62	0.960	62	0.962	62	0.961	50	0.952	26	0.957	26	0.960	33
23	RY_CNOT	DATA_REUP_PROB	IQP	0.0475	0.939	0.904	2519	0.529	2519	0.519	2557	0.531	2580	0.491	3173	0.508	1005	0.500	989	0.524	405
24	RX_RZ_Multi_CRZ	DATA_REUP_PROB	AngleY	0.9210	0.949	0.907	1100	0.915	1102	0.841	1110	0.937	1064	0.796	1671	0.495	556	0.487	544	0.951	93
25	RX_RZ_CRZPool	DATA_REUP_PROB	IQP	0.8288	0.926	0.870	1359	0.900	1445	0.861	1365	0.907	1374	0.796	1790	0.501	821	0.501	790	0.906	227
26	RX_RZ_Multi_CRZ	DATA_REUP_PROB	AngleY	1.1158	0.927	0.920	1167	0.927	1063	0.897	1113	0.932	1122	0.811	1598	0.503	568	0.506	550	0.923	93
27	RX_RZ_CRZPool	DATA_REUP_EXP	AngleY	2.6991	0.920	0.920	78	0.922	74	0.919	74	0.922	86	0.918	86	0.915	47	0.920	42	0.918	13
28	RX_RZ_CNOT	DATA_REUP_EXP	AngleY	0.0551	0.938	0.971	67	0.923	67	0.908	67	0.920	67	0.920	99	0.798	36	0.792	36	0.904	21
29	RX_RZ_Multi_CRX	DATA_REUP_EXP	AngleY	0.0700	0.907	0.712	1115	0.774	1200	0.694	1180	0.819	1165	0.694	1517	0.491	524	0.474	547	0.838	93
30	QNN_RY_CRX_pool	VQC_QNN_EXP	AngleX	1.0540	0.853	0.857	58	0.852	58	0.860	58	0.854	58	0.856	62	0.850	24	0.854	24	0.851	29
31	RX_RZ_CNOT	VQC_QNN_EXP	AngleY	0.0930	0.913	0.929	67	0.923	67	0.916	67	0.920	67	0.920	98	0.827	36	0.797	36	0.922	24
32	RY_CZ	VQC_QNN_EXP	Amplitude	0.0380	0.899	0.644	1983	0.648	1979	0.538	1978	0.706	1964	0.526	2509	0.496	661	0.522	674	0.652	594
33	QNN_RY_CNOT_pool	VQC_QNN_PROB	Amplitude	0.2120	0.909	0.749	1614	0.818	1656	0.621	1521	0.756	1406	0.545	1817	0.470	661	0.482	632	0.790	535
34	INV_QFT_U3_MODEL	VQC_QNN_PROB	IQP	0.1667	0.945	0.937	343	0.940	342	0.936	350	0.940	399	0.932	461	0.708	189	0.693	206	0.937	50
35	RY_CNOT	VQC_QNN_PROB	IQP	0.0380	0.933	0.872	378	0.914	383	0.846	377	0.904	382	0.717	506	0.500	176	0.517	142	0.850	72
36	RY_CNOT	VQC_QNN_PROB	AngleY	0.2970	0.907	0.902	105	0.902	106	0.904	105	0.904	105	0.889	142	0.804	52	0.814	52	0.899	36
37	RY_CRX	VQC_QNN_PROB	IQP	0.2750	0.906	0.897	355	0.911	365	0.891	355	0.902	359	0.897	442	0.728	174	0.736	175	0.898	64
38	RX_RZ_CNOT	VQC_QNN_PROB	AngleX	0.3167	0.888	0.896	67	0.890	67	0.893	67	0.891	67	0.893	88	0.875	36	0.880	36	0.887	24
39	H_CZ_RX	VQC_QNN_PROB	AngleY	0.2828	0.875	0.874	54	0.873	54	0.869	54	0.872	55	0.873	144	0.852	37	0.843	37	0.869	37
40	RY_RZ_CNOT	VQC_QNN_PROB	IQP	0.0671	0.959	0.852	399	0.881	398	0.841	379	0.879	386	0.741	505	0.578	123	0.534	146	0.877	58
41	RY_RZ_CNOT	DATA_REUP_EXP	IQP	0.1131	0.935	0.734	1279	0.795	1300	0.674	1281	0.838	1368	0.577	1873	0.490	721	0.490	718	0.858	197
42	RX_RZ_CRZPool	DATA_REUP_PROB	AngleZ	2.7730	0.930	0.927	88	0.928	73	0.925	69	0.928	73	0.921	97	0.927	24	0.925	20	0.928	13
43	RX_RZ_CRZPool	DATA_REUP_PROB	IQP	2.2790	0.923	0.902	1413	0.910	1415	0.908	1382	0.914	1361	0.903	2057	0.552	845	0.560	776	0.915	227
44	RX_RZ_CRZPool	DATA_REUP_PROB	IQP	1.9780	0.892	0.902	1381	0.905	1438	0.899	1435	0.905	1361	0.892	1812	0.595	785	0.583	811	0.906	227
45	RY_RZ_CNOT	DATA_REUP_EXP	AngleX	0.2600	0.940	0.924	180	0.928	133	0.915	177	0.925	192	0.899	182	0.913	22	0.915	22	0.919	21
46	RX_RZ_CRZPool	DATA_REUP_EXP	AngleZ	0.5350	0.892	0.937	76	0.941	69	0.940	74	0.941	78	0.936	110	0.934	28	0.936	28	0.934	13
47	QNN_RY_CRZ_pool	VQC_QNN_EXP	AngleY	1.5652	0.939	0.940	47	0.941	47	0.943	47	0.943	47	0.937	18	0.936	18	0.936	18	0.936	29
48	RY_CNOT	VQC_QNN_EXP	IQP	0.0131	0.912	0.786	377	0.829	380	0.727	375	0.817	381	0.540	503	0.501	155	0.501	168	0.736	72
49	RX_RZ_CNOT	DATA_REUP_PROB	AngleZ	0.0318	0.902	0.859	67	0.869	67	0.830	67	0.857	67	0.834	98	0.708	36	0.668	36	0.819	24
50	RY_CZ	DATA_REUP_PROB	AngleX	0.0869	0.902	0.859	404	0.869	403	0.830	403	0.857	398	0.834	823	0.708	92	0.668	92	0.819	92
51	RX_RZ_Multi_CRZ	DATA_REUP_PROB	AngleZ	0.5350	0.892	0.831	1192	0.874	1125	0.771	1120	0.877	1170	0.629	1613	0.500	571	0.433	541	0.912	93

TABLE I: Analysis of Variational Quantum Classification Models across Different Noisy Backends

VI. DISCUSSION

Our extensive experimentation across several variables such as datasets, model structures, devices, and ansatzes has proven that the results and interpretations presented in Section V are generalizable over a wide variety of Variational Quantum Classifiers.

The key observation from Table I is that what constitutes a noise-robust variational quantum classifier does not solely depend on depth or any single parameter but relies on other combinations of high average relative entropy amongst classes and low transpilation depth. This challenges the notion that a robust shallow variational circuit is one with a specific depth depending on the device’s capability.

We observed that several quantum circuits behaved differently on the same noisy devices, despite having similar transpilation depths. For instance, in the case of the noisy fake backend of the Sherbrooke device, we noted that a circuit with a depth of 2033 showed a higher accuracy difference of 0.4 between the simulation and the noisy device, while another circuit with a depth of 2236 exhibited a much smaller accuracy difference of just 0.029. This indicates that even with a greater depth, the accuracy difference can be minimal. The main distinction between these two circuits was their average relative entropy values. Many such observations can be derived from the data presented in Table I.

An additional observation from the graphs shown in Fig. 3, Fig. 4, and the log-DTSAE values of various devices in Section V is that each device has its own specific limits regarding the average relative entropy to transpilation depth ratio. This variation can be easily attributed to the differences in the noise characteristics of each of the noisy devices tested. We are currently exploring improved methods for calculating these values for noisy devices without requiring such extensive evaluations.

The highest observed average relative entropy between classes was 8.571, while the highest depth observed during experimentation was 20212.

No model with low accuracy difference between simulated and noisy devices was observed for Amplitude encoding, as the transpilation depth for this method was notably high across all the noisy backends. The lowest observed transpilation depth for an Amplitude embedding model was 515 for the IonQ Aria1, while IQM devices had a minimum value of 563, with the lowest value for IBM devices reaching 1335. These values are considerably high; for Amplitude embedding to be a viable option, the Average Relative entropy between classes needs to be extremely high.

Similar complexities for IQP embedding were observed, but weren’t as severe as for Amplitude, as with certain lower depth bounds and a high average relative entropy between classes, the accuracy difference could be curbed.

This brings about the problem with using these classical to quantum data encoding methods for practical Quantum Machine Learning implementation. Amplitude encoding can embed n features into $\log(n)$ qubits, but this ability is

questioned due to the implementation complexity, along with its expressibility of classical data. Better methods for state preparation could widely help in alleviating this issue.

There were other observations in the experiment that were associated with the transpilation procedure and the relative entropy during the data analysis. In a few observed models, the transpilation width, which is the number of qubits required to represent the circuit, increased due to the device structure being mapped to or the circuit design complexity. These lead to some values being skewed away from the norm, as showcased in Fig. 3 and 4.

During the initial training phase, we also observed the same class average relative entropy, difference class average relative entropy, and their association with the model’s accuracy. There isn’t a straight correlation between the model’s accuracy during simulation and the average entropy values. This leads to an important concern about how to train a model with a high average relative entropy between classes and high accuracy. Further work on this aspect is discussed in Section VIII and is currently under research.

As mentioned in Section V, we analyzed other metrics, such as the models’ predictive probability distributions, and found no correlation with noisy device performance; however, these distributions substantially contribute to the models’ accuracy. Skewed probability distribution in either of the classes leads to a model with less accuracy.

Results from the real quantum device reflect a similar effect to the fake noisy backends. While a little more interference from noise is observed on the real quantum devices, the overall effect on the results was not magnified and does not contradict the relation between depth and relative entropy analyzed in this manuscript. More evaluations for real quantum device evaluations are in progress.

Finally, based on the extensive experiments conducted on fake noisy backends, we propose some suggestions for the reproducibility of VQC models’ results on noisy devices. The values for ideal transpilation depth and ideal average relative entropy between classes highly depend on the noisy device in question and the acceptable accuracy difference concerning the problem being reproduced.

In Section V, we presented log-DTSAE graphs to showcase the dynamics of how these values influence each other, along with the accuracy difference, and it is clearly observed that these values are clearly device dependent and the noise channel associated with the model. But we suggest keeping the log-DTSAE ratio of models under 3.5 to have less deviation in accuracy. These values are bound to change with the progress in noise mitigation and betterment of gate fidelity.

VII. CONCLUSION

In this article, we examine two critical research gaps in Variational Quantum Classification (VQC) models: the varying effects of noise on model performance in noisy quantum devices, and the uncertainty in defining the ideal depth for a noise-robust shallow parameterized quantum circuits.

Using empirical evidence, we establish the correlation between average relative entropy, transpilation depth, and the reliability of Variational Quantum Classifiers (VQCs) operating on a noisy backend. Our analysis is based on a large number of experiments conducted across various VQC architectures, datasets, and noisy quantum backends.

We provide evidence that transpilation depth is not the only factor that determines noise resilience in shallow parameterized quantum circuits within VQCs. There is no single ideal depth value for any noisy device. Instead, a combination of the average relative entropy between classes and transpilation depth determines noise resilience in these models.

To determine the reproducibility factor of a VQC model on noisy hardware, we propose a new metric: log-DTSAE (the logarithm of the depth divided by the square root of the average relative entropy). This method is also equally important to analyze the ideal transpilation depth in relation to the average relative entropy between classes in a noisy quantum backend

This research presents a classical method to evaluate the reproducibility of Variational Quantum Circuit (VQC) results on Noisy Intermediate-Scale Quantum (NISQ) hardware without the need for explicit executions on quantum devices. It lays the groundwork for scalable and reliable quantum machine learning (QML) procedures in noisy environments. Additionally, this article opens the door for further exploration of various other problems, which are discussed in the next section VIII.

VIII. FUTURE WORK

The observations made during the implementation of this study, along with the noted relationship between noise robustness and average relative entropy in variational circuits, suggest several promising directions for future research:

- Develop computationally efficient methods to estimate log-DTSAE for new noisy quantum backends without requiring extensive empirical evaluations.
- Investigate warm-start strategies for initializing VQC models that promote higher average relative entropy between classes and improved robustness to noise.
- Explore training methodologies for Variational Quantum models that directly optimize average relative entropy on noisy quantum hardware.
- Analyze the scalability of the proposed relative entropy-based framework with increasing qubit counts and circuit complexity.
- Determining the ideal combination of multiple optimizer structures for faster minima approximation.
- Study the impact of circuit compression techniques on models with low average relative entropy, particularly in improving their reproducibility on noisy backends.

IX. ACKNOWLEDGMENT

We would like to express our special thanks to Valter Uotila for his valuable comments on the research and the creation of this manuscript. We also extend our gratitude to Ilmo

Salmenperä, Frans Perkkola, Tung Bui Dang, and Leo Becker for their insightful discussions and guidance during the early phases of the research.

X. DATA AND CODE REPOSITORIES

- VQC-QNN Training and Testing Code and Data [38]: https://github.com/AakashShindeHelsinki/VQC_QNN_QML_Model_Training_and_Benchmarking
- Data-Reupload Training and Testing Code and Result Data [39]: https://github.com/AakashShindeHelsinki/DataReupload_QML_Training_and_Benchmarking
- QML model testing on noisy devices runs, transpilation depth generation, depth-entropy analysis, and data processing [40]: https://github.com/AakashShindeHelsinki/NoisyDev_Testing_and_Ent_Data_Processing

XI. APPENDIX

Examples of all the circuit structures used in computation and experiment are available on the following GitHub repository: https://github.com/AakashShindeHelsinki/Quantum_Circuit_Diagrams_for_RelEnt_analysis

REFERENCES

- [1] M. Cerezo, A. Arrasmith, R. Babbush, S. C. Benjamin, S. Endo, K. Fujii, J. R. McClean, K. Mitarai, X. Yuan, L. Cincio, *et al.*, “Variational quantum algorithms,” *Nature Reviews Physics*, vol. 3, no. 9, pp. 625–644, 2021.
- [2] K. Sharma, S. Khatri, M. Cerezo, and P. J. Coles, “Noise resilience of variational quantum compiling,” *New Journal of Physics*, vol. 22, no. 4, p. 043006, 2020.
- [3] T. A. Brun, “Quantum error correction,” *arXiv preprint arXiv:1910.03672*, 2019.
- [4] S. Wang, E. Fontana, M. Cerezo, K. Sharma, A. Sone, L. Cincio, and P. J. Coles, “Noise-induced barren plateaus in variational quantum algorithms,” *Nature communications*, vol. 12, no. 1, p. 6961, 2021.
- [5] K. Phalak and S. Ghosh, “Shot optimization in quantum machine learning architectures to accelerate training,” *IEEE Access*, vol. 11, pp. 41514–41523, 2023.
- [6] B. Khanal and P. Rivas, “Evaluating the impact of noise on variational quantum circuits in nisq era devices,” in *2023 Congress in Computer Science, Computer Engineering, & Applied Computing (CSCE)*, pp. 1658–1664, IEEE, 2023.
- [7] E. Fontana, N. Fitzpatrick, D. M. Ramo, R. Duncan, and I. Rungger, “Evaluating the noise resilience of variational quantum algorithms,” *Physical Review A*, vol. 104, no. 2, p. 022403, 2021.
- [8] T. Ahmed, M. Kashif, A. Marchisio, and M. Shafique, “A comparative analysis and noise robustness evaluation in quantum neural networks,” *Scientific Reports*, vol. 15, no. 1, p. 33654, 2025.
- [9] A. Bärligea, B. Poggel, and J. M. Lorenz, “Scalability challenges in variational quantum optimization under stochastic noise,” *Physical Review A*, vol. 112, no. 3, p. 032407, 2025.
- [10] E. Adermann, H. Suzuki, and M. Usman, “Variational quantum machine learning with quantum error detection,” *Quantum Machine Intelligence*, vol. 8, no. 1, p. 1, 2026.
- [11] G. De Palma, M. Marvian, C. Rouzé, and D. S. França, “Limitations of variational quantum algorithms: a quantum optimal transport approach,” *PRX Quantum*, vol. 4, no. 1, p. 010309, 2023.
- [12] T. Hur, L. Kim, and D. K. Park, “Quantum convolutional neural network for classical data classification,” *Quantum Machine Intelligence*, vol. 4, no. 1, p. 3, 2022.
- [13] S. Mondal and A. K. Dutta, “Relative entropy-based training of quantum neural networks,” *IEEE Transactions on Quantum Engineering*, vol. 7, pp. 1–14, 2025.
- [14] K. Tsuda, “Machine learning with quantum relative entropy,” in *Journal of Physics: Conference Series*, vol. 143, p. 012021, 2009.

- [15] J. Biamonte, P. Wittek, N. Pancotti, P. Rebentrost, N. Wiebe, and S. Lloyd, "Quantum machine learning," *Nature*, vol. 549, no. 7671, pp. 195–202, 2017.
- [16] Z. Goldfeld, D. Patel, S. Sreekumar, and M. M. Wilde, "Quantum neural estimation of entropies," *Physical Review A*, vol. 109, no. 3, p. 032431, 2024.
- [17] M. Shin, J. Lee, and K. Jeong, "Estimating quantum mutual information through a quantum neural network: M. shin et al.," *Quantum Information Processing*, vol. 23, no. 2, p. 57, 2024.
- [18] J. Bowles, S. Ahmed, and M. Schuld, "Better than classical? the subtle art of benchmarking quantum machine learning models," *arXiv preprint arXiv:2403.07059*, 2024.
- [19] T. Hubregtsen, J. Pichlmeier, P. Stecher, and K. Bertels, "Evaluation of parameterized quantum circuits: on the relation between classification accuracy, expressibility, and entangling capability," *Quantum Machine Intelligence*, vol. 3, no. 1, p. 9, 2021.
- [20] S. Sim, P. D. Johnson, and A. Aspuru-Guzik, "Expressibility and entangling capability of parameterized quantum circuits for hybrid quantum-classical algorithms," *Advanced Quantum Technologies*, vol. 2, no. 12, p. 1900070, 2019.
- [21] P. Bermejo, P. Braccia, M. S. Rudolph, Z. Holmes, L. Cincio, and M. Cerezo, "Quantum convolutional neural networks are (effectively) classically simulable," *arXiv preprint arXiv:2408.12739*, 2024.
- [22] N. Schetakakis, P. Bonfini, N. Alisoltani, K. Blazakis, S. I. Tsintzos, A. Askitopoulos, D. Aghamalyan, P. Fafoutellis, and E. I. Vlahogianni, "Data re-uploading in quantum machine learning for time series: application to traffic forecasting," *arXiv preprint arXiv:2501.12776*, 2025.
- [23] M. M. Wilde, "From classical to quantum shannon theory," *arXiv preprint arXiv:1106.1445*, 2011.
- [24] I. M. Guyon, "Design of experiments for the nips 2003 variable selection benchmark," 2003.
- [25] "Generated datasets — scikit-learn.org." https://scikit-learn.org/stable/datasets/sample_generators.html. [Accessed 27-02-2026].
- [26] B. Barr, K. Xu, C. T. Silva, E. Bertini, R. Reilly, C. B. Bruss, and J. D. Wittenbach, "Towards ground truth explainability on tabular data," *ArXiv*, vol. abs/2007.10532, 2020.
- [27] S. Goldt, M. Mézard, F. Krzakala, and L. Zdeborová, "Modeling the influence of data structure on learning in neural networks: The hidden manifold model," *Physical Review X*, 2019.
- [28] S. Buchanan, D. Gilboa, and J. Wright, "Deep networks and the multiple manifold problem," *arXiv preprint arXiv:2008.11245*, 2020.
- [29] O. Zang, G. Barrué, and T. Quertier, "Benchmarking data encoding methods in quantum machine learning," *arXiv preprint arXiv:2505.14295*, 2025.
- [30] M. Monnet, N. Chaabani, T.-A. Drăgan, B. Schachtner, and J. M. Lorenz, "Understanding the effects of data encoding on quantum-classical convolutional neural networks," in *2024 IEEE International Conference on Quantum Computing and Engineering (QCE)*, vol. 1, pp. 1436–1446, IEEE, 2024.
- [31] V. Havlíček, A. D. Córcoles, K. Temme, A. W. Harrow, A. Kandala, J. M. Chow, and J. M. Gambetta, "Supervised learning with quantum-enhanced feature spaces," *Nature*, vol. 567, no. 7747, pp. 209–212, 2019.
- [32] V. Uotila, I. Salmenperä, L. Becker, A. Meijer van de Griend, A. R. Shinde, and J. K. Nurminen, "Perspectives on utilization of measurements in quantum algorithms," in *2025 IEEE International Conference on Quantum Software (QSW)*, 2025.
- [33] J. Seo, "Multivariate unbounded quantum regression via log-ratio probabilities mitigating barren plateaus," *IEEE Access*, vol. 14, pp. 4877–4885, 2026.
- [34] V. Bergholm, J. Izaac, M. Schuld, C. Gogolin, S. Ahmed, V. Ajith, M. Sohaib Alam, G. Alonso-Linaje, B. AkashNarayanan, A. Asadi, J. M. Arrazola, U. Azad, S. Banning, C. Blank, T. R. Bromley, B. A. Cordier, J. Ceroni, A. Delgado, O. Di Matteo, A. Dusko, T. Garg, D. Guala, A. Hayes, R. Hill, A. Ijaz, T. Isaacsson, D. Ittah, S. Jahangiri, P. Jain, E. Jiang, A. Khandelwal, K. Kottmann, R. A. Lang, C. Lee, T. Loke, A. Lowe, K. McKiernan, J. J. Meyer, J. A. Montañez-Barrera, R. Moyard, Z. Niu, L. J. O’Riordan, S. Oud, A. Panigrahi, C.-Y. Park, D. Polatajko, N. Quesada, C. Roberts, N. Sá, I. Schoch, B. Shi, S. Shu, S. Sim, A. Singh, I. Strandberg, J. Soni, A. Száva, S. Thabet, R. A. Vargas-Hernández, T. Vincent, N. Vitucci, M. Weber, D. Wierichs, R. Wiersema, M. Willmann, V. Wong, S. Zhang, and N. Killoran, "PennyLane: Automatic differentiation of hybrid quantum-classical computations," *arXiv e-prints*, p. arXiv:1811.04968, Nov. 2018.
- [35] "OpenQASM Live Specification — OpenQASM Live Specification documentation — openqasm.com." <https://openqasm.com/>. [Accessed 28-02-2026].
- [36] A. Javadi-Abhari, M. Treinish, K. Krsulich, C. J. Wood, J. Lishman, J. Gacon, S. Martiel, P. D. Nation, L. S. Bishop, A. W. Cross, B. R. Johnson, and J. M. Gambetta, "Quantum computing with Qiskit," 2024.
- [37] J. Wang, "An intuitive tutorial to gaussian process regression," *Computing in Science & Engineering*, vol. 25, no. 4, pp. 4–11, 2023.
- [38] A. R. Shinde, "PQCs and QNN (Probabilistic and Expectation Value Measures) Models for Quantum Machine Learning Testing and Data Processing." https://github.com/AakashShindeHelsinki/VQC_QNN_QML_Model_Training_and_Benchmarking, Mar. 2026.
- [39] A. R. Shinde, "Data Reupload (Probabilistic and Expectation Value measure) Models for Quantum Machine Learning Testing and Data Processing." https://github.com/AakashShindeHelsinki/DataReupload_QML_Training_and_Benchmarking, Mar. 2026.
- [40] A. R. Shinde, "QML model testing on noisy devices, depth-entropy analysis and data processing ." https://github.com/AakashShindeHelsinki/NoisyDev_Testing_and_Ent_Data_Processing, Mar. 2026.